PERGAMON

International Journal of Solids and Structures 40 (2003) 6547–6565

INTERNATIONAL JOURNAL OF SOLIDS and STRUCTURES

www.elsevier.com/locate/ijsolstr

Buckling of stochastically heterogeneous beams, using a functional perturbation method

Eli Altus *, Essam M. Totry

Faculty of Mechanical Engineering, Technion, Israel Institute of Technology, Haifa 32000, Israel

Abstract

The buckling load and its probabilistic nature (average and variance) of Bernoulli beams with stochastic material (bending stiffness) properties is derived analytically by a new functional perturbation method (FPM). A buckling shape function is assumed, based on the homogeneous solution and additional terms to account for the morphology effects. The buckling load in the transcendental equation is treated as a functional of the bending modulus (stiffness or compliance) field. Applying a functional perturbation to the above equation, the buckling load is found analytically to any desired degree of accuracy, as a function of material morphology. The FPM is executed using both stiffness and compliance statistical data. The impact of each of the two data sources on the solution accuracy is examined, showing that compliance based solutions are accurate for small correlation lengths. Statically indeterminate problems can be treated with no additional effort. An example of a simply supported beam is solved in detail. Comparison with previous studies, where stochastic finite element and Monte Carlo simulation were used, showed the relative accuracy and insight capabilities of the method. The clamped-free case is also studied to demonstrate that symmetry conditions, used for homogeneous beams to find the buckling load on the basis of a simply supported case, are not valid for heterogeneous beams.

Keywords: Beams; Heterogeneity; Stochastic; Buckling; Perturbation; Functional analysis

1. Introduction

Buckling problems of heterogeneous structures (beams, plates) can be divided into two types. The first concerns a structure with a cross sectional heterogeneity, which is a type of ''imperfection'' for which a transverse displacement is present even for small loads. Failure criteria may be governed by allowable deflections (essentially a bending problem). The second type is a problem related to longitudinal heterogeneity, which changes the buckling load itself (i.e., eigenvalue problem). Interestingly, most of the studies in the literature (see a comprehensive review by Elishakoff, 2000) are dedicated to the first type, probably because of its major importance in engineering design. However, the present study is concerned with the second type. External loads are not stochastic, although reaction forces are generally random too.

* Corresponding author. Tel.: +972-4-829-3157; fax: +972-4-832-4533.
E-mail addresses: altus@tx.technion.ac.il (E. Altus), totryess@tx.technion.ac.il (E.M. Totry).

0020-7683/$ - see front matter © 2003 Elsevier Ltd. All rights reserved.
doi:10.1016/S0020-7683(03)00394-9

Solutions for the buckling loads of longitudinally heterogeneous beams can be either analytical (usually by some perturbation method), numerical (Monte Carlo finite element simulation) or a mixture of both (stochastic finite element, SFE). In addition, it is important whether the problem is statically determinate or not, since indeterminacy causes the reaction forces (and therefore the buckling loads) to be functionally (and statistically) dependent on the stiffness morphology.

In a pioneering work, Shinozuka and Astill (1972) used the classical perturbation method to analyze the stability and vibration problem of beam columns. In their study, the average and variance of each solution for the eigenvalue problem, was related only to the corresponding deflection mode of the homogeneous solution.

Ramu and Ganesan (1994) studied the stability and vibration characteristics of beams with stochastic material properties and loading, using energy principle and perturbation methods, and assuming again a "homogeneous" shape functions. Thus, the average buckling load was found to be independent of the stiffness correlation length (roughly the "grain size").

Garrett (1992) used a Monte Carlo simulation (MCS, by finite elements) to study the morphology effect on the buckling load. Zhang and Ellingwood (1995) used the SFE method, where the continuous random fields of material properties are described by a given series of orthogonal functions. Thus, the correlation length effect on the buckling load statistics could be incorporated.

Graham and Deodatis (1998, 2001), and Graham and Siragy (2001), solved the eigenvalue variability problem as part of a more general SFE method using variability response functions and also found bounds on the buckling load variability.

The inverse buckling method (Elishakoff, 2001) is a different approach to the problem of heterogeneous beams, where specific stiffness functions are considered, for which an exact buckling solution is available. Development of this method for stochastic heterogeneity is still in demand.

In this study, a functional perturbation method (FPM), previously developed for calculating the deflection (Altus, 2001) and strength (Altus and Givli, 2002) of stochastically heterogeneous beams, is further generalized to treat buckling problems. The statistical features of the buckling load are obtained analytically, as a function of the material morphology characteristics i.e., multiple point probabilities of the stiffness or compliance functions. The accuracy and validity of the method is checked by comparison with the studies of Garrett (1992) and Zhang and Ellingwood (1995).

2. Notations, definitions and mathematical operations

In this chapter, a set of notations and operations used in the text are introduced. Section 2.1 deals with probability and morphology, and Section 2.2 is related to functional algebra.

2.1. Probability symbols

Let E and I be the non-uniform Young's modulus and cross sectional inertia, respectively, the bending stiffness morphology is defined by

$$K(x) = E(x)I(x). \tag{2.1}$$

$K(x)$ is considered as a stochastic and statistically homogeneous field. The following common notations will be used in the sequel:

$$K' = K - \langle K \rangle; \quad \overline{K} = \frac{K}{\langle K \rangle}; \quad \overline{K}' = \frac{K'}{\langle K \rangle}, \tag{2.2}$$

where $\langle()\rangle$, $()'$ and $\overline{()}$ are notations for the statistical average, deviation from the mean and normalization (usually to some average value). Thus $\overline{()}'$ is the normalized deviation. Also,

$$\mathrm{Var}(K) = \langle (K')^2 \rangle; \quad \mathrm{Var}(\overline{K}) = \frac{\mathrm{Var}(K)}{\langle K \rangle^2} \tag{2.3}$$

and

$$\rho_K = [\mathrm{Var}(\overline{K})]^{1/2}, \tag{2.4}$$

is the coefficient of variation (COV) of K.

The two-point stiffness correlation function is defined as:

$$\langle K'K' \rangle \equiv \langle K'(x)K'(X) \rangle = \langle K'(x)K'(x+h) \rangle = \langle K'(x)K'(x-h) \rangle, \tag{2.5}$$

where x and X are coordinates along the beam and $h = |x - X|$.

For random morphology of "grain like" materials, we define an effective "correlation length (distance)" λ by:

$$\int_0^\infty \langle K'(x)K'(x+h) \rangle \, \mathrm{d}h = \lambda \langle K'(x)^2 \rangle = \lambda \, \mathrm{Var}(K), \tag{2.6}$$

which is in the order of the grain size. Note that (2.6) is one way of decoupling material properties ($\mathrm{Var}(K)$) from geometry characteristics (λ). One of the convenient, frequently used correlation functions has the exponential form, which yields:

$$\langle \overline{K}'\overline{K}' \rangle = \langle (\overline{K}')^2 \rangle \exp\left[-\frac{|X - x|}{\lambda} \right]. \tag{2.7}$$

This form will also be used in the examples below.

2.2. Functional symbols and operations

First we define the Dirac singularity function by the functional self derivative (Beran, 1968):

$$\delta(x_1 - x_2) = \frac{\delta K(x_1)}{\delta K(x_2)} = \delta K_{,K}. \tag{2.8}$$

The notation of the δ symbol is common for both the Dirac function and functional derivatives. However, this duplicity does not cause any confusion. Thus, by (2.8):

$$K(x_1) = \int \delta(x_1 - x_2) K(x_2) \, \mathrm{d}x_2; \quad K = \delta * K, \tag{2.9}$$

where $(*)$ is the convolution symbol. Thus, $K(x_1)$ is a functional of $K(x_2)$.

A simple integration is written by a functional unit symbol **1**:

$$\int K(x) \, \mathrm{d}x = \mathbf{1} * K = K * \mathbf{1}. \tag{2.10}$$

Thus, **11** is a two variable unit function such that

$$\mathbf{1} * \mathbf{1} = x; \quad \delta * \mathbf{1} = \mathbf{1}. \tag{2.11}$$

Two functions $K(x)$ and $S(x)$, written next to each other without any symbol in between, are considered as multiplied "externally", i.e.,

$$KS \equiv K(x_1)S(x_2). \tag{2.12}$$

Multiplication of two single variable functions at the same point is denoted by an "empty dot":

$$K \circ S \equiv K(x)S(x); \quad K^2 \equiv K \circ K \tag{2.13}$$

and for multivariable functions:

$$K\delta \equiv K(x_1)\delta(x_2 - x_3); \quad K \circ \delta \equiv K(x_1)\delta(x_1 - x_2), \tag{2.14}$$

which is similar to scalar products in tensors.

Consider a parameter P, which is a functional of $K(x)$. The functional derivatives are generally written as

$$\frac{\delta P}{\delta K} \equiv \frac{\delta P\{K(x_1)\}}{\delta K(x_2)} \equiv P_{,K}; \quad \frac{\delta^2 P}{\delta K\,\delta K} \equiv \frac{\delta^2 P\{K(x_1)\}}{\delta K(x_2)\,\delta K(x_3)} \equiv P_{,KK}, \tag{2.15}$$

where ( ) and { } are designated for functions and functionals, respectively. Note that multiple derivatives are also "external".

Now consider a parameter P, which is a functional of $K(x)$, as follows:

$$P = P\{K\} = \int F(x, K(x))\,\mathrm{d}x, \tag{2.16}$$

Thus, P is a functional of K through F, which is a function of K. The functional derivative of P with respect to K is:

$$\frac{\delta P}{\delta K} = \frac{\delta P\{K(x)\}}{\delta K(x_1)} = \int \frac{\partial F}{\partial K(x)} \frac{\delta K(x)}{\delta K(x_1)}\,\mathrm{d}x = \int \frac{\partial F}{\partial K(x)}\delta(x - x_1)\,\mathrm{d}x = \left.\frac{\partial F}{\partial K}\right|_{x=x_1} = \frac{\partial F(x_1, K(x_1))}{\partial K(x_1)} = F_{,\partial K}\,. \tag{2.17}$$

For convenience, we use the convolution notation and write the above as:

$$P_{,\delta K} = F_{,K} * K_{,\delta K} = F_{,K} * \delta = F_{,K}, \tag{2.18}$$

where $(\,)_{,K}$, $(\,)_{,\delta K}$ and $(\,)_{,\partial K}$ are for "general", functional and "regular" derivatives, respectively. However, in cases where there is only one way of interpretation, the first symbol will be used for convenience. There is also the problem of distinguishing between a partial functional derivative and a regular partial derivative, but we will not assign additional symbols to avoid confusion.

Finally, multiple convolutions of functions of two or more variables are written consistently. For example:

$$\delta K * P_{,KK} * \delta K \equiv \delta K(x_1) * \frac{\delta^2 P}{\delta K(x_1)\,\delta K(x_2)} * \delta K(x_2). \tag{2.19}$$

Since $P_{,KK}$ is symmetric with respect to its two functional variables, we can write also

$$P_{,KK} * *\delta K\,\delta K \equiv \delta K * P_{,KK} * \delta K. \tag{2.20}$$

Unless otherwise specified, convolutions ($*$) are performed along the length of the beam, i.e., from 0 to 1.

3. Buckling loads by the functional perturbation method—general procedures

In this section, the FPM, introduced by Altus (2001) for beam bending, is generalized for the study of stability problems. Buckling loads are obtained analytically. The FPM procedure for a simple example is used as a demonstration in Section (3.1), which is generalized in Section (3.2) to a class of compressive loading and boundary conditions.

3.1. Average and variance for the buckling load of a simply supported beam

Consider a beam of length L, simply supported at both ends, and loaded by a compression force P. $E(x)$ and $I(x)$ are the non-uniform modulus and inertia, respectively. The bending stiffness (K) and compliance (S) are defined as follows:

$$K(x) = EI(x); \quad S(x) = (K(x))^{-1}, \tag{3.1}$$

where x is the normalized (by L) longitudinal coordinate, i.e., $(0 < x < 1)$.

Now, assume a buckling deflection of the form:

$$w(x) = \sum_{k=1}^{n} A_k w_k(x), \tag{3.2}$$

where $w_k(x)$ are a set of prescribed shape functions which obey the boundary conditions:

$$w_k(0) = w_k(1) = 0; \quad w_{k,xx}(0) = w_{k,xx}(1) = 0. \tag{3.3}$$

A_k are shape coefficients to be determined. During buckling, the moment distribution $M(x)$ along the beam is simply:

$$M(x) = Pw(x), \tag{3.4}$$

where P is the buckling load. The bending strain energy U during buckling is:

$$U = \int_0^1 \frac{M^2}{2K(x)}\,\mathrm{d}x = \frac{1}{2}M^2 * K^{-1} \tag{3.5}$$

and the external work done by the force P during buckling is:

$$T = \int_0^1 \frac{P}{2}(w_{,x})^2\,\mathrm{d}x = \frac{1}{2}P(w_{,x})^2 * \mathbf{1}. \tag{3.6}$$

Inserting (3.2) in (3.5) and (3.6), the total potential energy of the system Π is:

$$\Pi = U - T = \tfrac{1}{2}\Omega_{km}A_kA_m, \tag{3.7}$$

where

$$\Omega_{km} = \Omega_{mk} = P\int_0^1 \left(P\frac{w_k \circ w_m}{K(x)} - w_{k,x} \circ w_{m,x}\right)\mathrm{d}x = P[P(w_k \circ w_m) * K^{-1} - (w_{k,x} \circ w_{m,x}) * \mathbf{1}]. \tag{3.8}$$

The critical buckling load P_K, associated with the stiffness K is found by:

$$\frac{\partial \Pi}{\partial A_n} = 0 \rightarrow \tfrac{1}{2}\Omega_{km}(\delta_{kn}A_m + A_k\delta_{mn}) = \tfrac{1}{2}[\Omega_{nm}A_m + \Omega_{kn}A_k] = \Omega_{nm}A_m = 0, \tag{3.9}$$

where the symmetry of Ω has been used. Therefore, the critical buckling load P_K is found by solving the equation:

$$D = \det(\mathbf{\Omega}) = 0. \tag{3.10}$$

So far, Eqs. (3.1)–(3.10) described the elementary "energy based" approximate solution for the buckling load. When the beam is non-uniform, D in (3.10) can be considered as a functional of K, and a function of P, which itself is a functional of K, i.e.,

$$D = D(\{K\}, P\{K\}) = 0. \tag{3.11}$$

Our first goal is to find the average buckling load for the stochastically heterogeneous beam. First note that

$$P = P(\langle K\rangle) + P_{,K}\Big|_{\langle K\rangle} * K' + \tfrac{1}{2}P_{,KK}\big|_{\langle K\rangle} * *K'K' + \cdots, \tag{3.12}$$

where $K' = \delta K$ for perturbation around $\langle K\rangle$. Averaging (3.12) yields:

$$\langle P\rangle = P(\langle K\rangle) + \tfrac{1}{2}P_{,KK}\big|_{\langle K\rangle} * *\langle K'K'\rangle + \cdots. \tag{3.13}$$

Since (3.11) is valid for any $K(x)$, it is specifically true for $K = \langle K\rangle$:

$$D(\langle K\rangle, P\langle K\rangle) = 0. \tag{3.14}$$

Moreover, all functional derivatives of D, with respect to K also vanish. The first functional derivative is:

$$D_{,K} = \frac{\delta D(x)}{\delta K(x_1)} = \frac{\partial D(x)}{\partial K(x_1)} + \frac{\partial D}{\partial P}\frac{\delta P(x)}{\delta K(x_1)} = D_{,\partial K} + D_{,P}P_{,K} = 0. \tag{3.15}$$

By the same procedure, the second functional derivative is:

$$D_{,KK} = (D_{,K})_{,K} = D_{,\partial K,\partial K} + 2D_{,\partial K,P}P_{,K} + D_{,PP}P_{,K}P_{,K} + D_{,P}P_{,KK} = 0, \tag{3.16}$$

where all values in (3.15) and (3.16) are at $K = \langle K\rangle$.

Thus, we can find $P(\langle K\rangle)$ from (3.14), insert in (3.15) and obtain $P_{,K}(\langle K\rangle)$, insert in (3.16) to obtain $P_{,KK}(\langle K\rangle)$ etc. Once these functional derivatives are known, they are inserted in (3.13) to obtain an explicit approximation for $\langle P\rangle$.

Our next step is to calculate $\mathrm{Var}(P)$, i.e.,

$$\mathrm{Var}(P) = \langle P^2\rangle - \langle P\rangle^2. \tag{3.17}$$

Inserting (3.12) in (3.17), using the relation $\langle K'\rangle = 0$ and rearranging, we obtain (notice the symmetrical form):

$$\mathrm{Var}(P) = P_{,K}|_{\langle K\rangle} * \langle K'K'\rangle * P_{,K}|_{\langle K\rangle} + \mathrm{O}(K'^3). \tag{3.18}$$

Therefore, once we find $P_{,K}$ from (3.14) and (3.15), $\mathrm{Var}(P)$ is explicitly found from (3.18).

3.2. Generalization to other loading geometries

In the more general case, when the beam is statically indeterminate, the procedure is very similar. Take for example the case of a beam which is clamped on both sides, or when more than two support points are present. Assuming a deflection function, which fulfills all geometric boundary conditions as above, we obtain the following form for the internal bending moment:

$$M(x) = PA_i w_i(x) + R_I g_I(x); \quad i \in \{1\text{–}n\},\ I \in \{1\text{–}N\}, \tag{3.19}$$

where $\mathbf{R}$ is a generalized force vector of the boundary constraints and $\mathbf{g}$ contains the specific (given, non-random) geometry details of the constraints. Note that $n \neq N$.

Inserting (3.19) in (3.7), the minimum potential energy principle renders:

$$\frac{\partial \Pi}{\partial A_j} = \Omega_{ji}^{(AA)}A_i + \Omega_{jI}^{(AR)}R_I = 0, \tag{3.20}$$

where

$$\Omega_{ji}^{(AA)} = P^2\int \frac{w_j w_i}{K}\,\mathrm{d}x; \quad \Omega_{jI}^{(AR)} = P\int \frac{w_j g_I}{K}\,\mathrm{d}x \tag{3.21}$$

and

$$\frac{\partial \Pi}{\partial R_J} = \Omega_{Ji}^{(RA)} A_i + \Omega_{JI}^{(RR)} R_I = 0, \tag{3.22}$$

where

$$\Omega_{Ji}^{(RA)} = P \int \frac{g_J w_i}{K}\,\mathrm{d}x; \quad \Omega_{JI}^{(RR)} = \int \frac{g_J g_I}{K}\,\mathrm{d}x. \tag{3.23}$$

Thus, similar to (3.10), the buckling load is obtained from:

$$D = \det(\mathbf{\Omega}) = 0; \quad [\Omega] = \begin{bmatrix} \Omega_{ji}^{(AA)} & \Omega_{jI}^{(AR)} \\ \Omega_{Ji}^{(RA)} & \Omega_{JI}^{(RR)} \end{bmatrix}, \tag{3.24}$$

where Ω is a symmetric $(n+N)\times(n+N)$ matrix.

4. Example: simply supported beam

The following example is chosen since its solution has been studied extensively in the literature by Garrett (1992), using finite element MCS, and by Zhang and Ellingwood (1995), using SFE. We base our deflection shape function $(w(x))$ on the exact shape of the homogeneous case. The reason is that this shape coincides with the exact solution for the two non-homogeneous limit cases where the correlation distance is very small or very large relative to the length of the beam. The above choice is applicable to any heterogeneous structure. Thus we assume a shape of the form:

$$w(x) = A_1 w_1(x) + A_2 w_2(x) = A_1 \sin(\pi x) + A_2 \sin(n\pi x). \tag{4.1}$$

The second term serves as a "sensor" for studying the effect of (n) on the accuracy of the solution. Since each term in (4.1) adds a degree of freedom to the beam, it is expected that the solution for the buckling load will decrease as we use more terms, when the minimum potential energy principle is applied. Therefore, we will choose the specific n, which yields the minimal buckling load. Since the first term corresponds to the exact solution for the homogeneous case, the "best" n will also be the one for which the effect of w_2 is maximal. Of course, more terms can be added when necessary. Moreover, in more complicated cases, a numerical solution for the homogeneous case can be found first, and then its shape function can be used as the first term in (4.1).

The internal bending moment distribution $M(x)$ along the beam is:

$$M(x) = Pw(x). \tag{4.2}$$

It is obvious from (4.1) and (4.2) that the boundary conditions for both the deflections and the bending moments are satisfied automatically. Inserting (4.1) and (4.2) in (3.5) and (3.6) and following the steps through (3.10) yields:

$$P\begin{bmatrix} PK^{-1} * w_1^2 - \pi^2/2 & PK^{-1} * (w_1 \circ w_2) \\ PK^{-1} * (w_1 \circ w_2) & PK^{-1} * w_2^2 - n^2\pi^2/2 \end{bmatrix} \begin{Bmatrix} A_1 \\ A_2 \end{Bmatrix} = 0. \tag{4.3}$$

A solution of (4.3) yields a quadratic equation for the buckling load P:

$$P^2[(K^{-1} * w_1^2)(K^{-1} * w_2^2) - (K^{-1} * (w_1 \circ w_2))^2] - P\frac{\pi^2}{2}[n^2(K^{-1} * w_1^2) + (K^{-1} * w_2^2)] + \frac{n^2\pi^4}{4} = 0. \tag{4.4}$$

To calculate the buckling load by the FPM, we follow the procedure outlined in Section 3. Using (3.14) we substitute $K = \langle K \rangle$ in (4.4) and solve for P, obtaining the two solutions:

$$P_1 = P_{\langle K \rangle} = \pi^2 \langle K \rangle; \quad P_2 = n^2\pi^2 \langle K \rangle. \tag{4.5}$$

These are the Euler solutions, as expected. Using (4.5a) as the critical load for the homogeneous solution in (3.15), we obtain:

$$P_{,K}|_{\langle K\rangle} = \left.\frac{\delta P}{\delta K}\right|_{\langle K\rangle} = -\left.\frac{D_{,\partial K}}{D_{,P}}\right|_{\langle K\rangle}, \tag{4.6}$$

where

$$D_{,\partial K} = P^2\left[2(K^{-2}\circ w_1\circ w_2)(K^{-1} * (w_1\circ w_2)) - (K^{-2}\circ w_1^2)(K^{-1} * w_2^2) - (K^{-2}\circ w_2^2)(K^{-1} * w_1^2)\right] + P\frac{\pi^2}{2}\left[(K^{-2}\circ w_2^2) + n^2(K^{-2}\circ w_1^2)\right] \tag{4.7}$$

and

$$D_{,P} = 2P[(K^{-1} * w_1^2)(K^{-1} * w_2^2) - (K^{-1} * (w_1\circ w_2))^2] - \frac{\pi^2}{2}[K^{-1} * (n^2 w_1^2 + w_2^2)]. \tag{4.8}$$

Substituting $K = \langle K\rangle$ in (4.7) and (4.8) and inserting in (4.6), yields simply:

$$P_{,K}|_{\langle K\rangle} = 2\pi^2 w_1^2, \tag{4.9}$$

where w_2 cancels out. Similarly, solving for $P_{,KK}$ from (3.16) using (4.7) and (4.8) and substituting $K = \langle K\rangle$ again (details are not given here) yields:

$$P_{,KK} = \left.\frac{\delta^2 P}{\delta K\,\delta K}\right|_{\langle K\rangle} = \frac{4\pi^2}{\langle K\rangle}\left[2w_1^2 w_1^2 - w_1^2\circ\delta - \frac{2}{n^2-1}(w_1\circ w_2)(w_1\circ w_2)\right], \tag{4.10}$$

where the relations and operations defined in Section 2 have been used.

Finally, inserting (4.5a) and (4.10) in (3.13), and noticing that

$$(w_1^2\circ\delta) * *\langle \overline{K}'\overline{K}'\rangle = (w_1^2) * \langle \overline{K}'^2\rangle = [(w_1^2) * 1]\langle \overline{K}'^2\rangle = \tfrac{1}{2}\langle \overline{K}'^2\rangle, \tag{4.11}$$

we obtain:

$$\langle \bar{P}_K\rangle = \frac{\langle P_K\rangle}{P_{\langle K\rangle}} = 1 - \mathrm{Var}(\overline{K}) + 4w_1^2 * \langle \overline{K}'\overline{K}'\rangle * w_1^2 - \frac{4}{n^2-1}(w_1\circ w_2) * \langle \overline{K}'\overline{K}'\rangle * (w_1\circ w_2). \tag{4.12}$$

From (3.18) and (4.9) we have also

$$\mathrm{Var}(\bar{P}_K) \cong 4w_1^2 * \langle \bar{K}'\bar{K}'\rangle * w_1^2. \tag{4.13}$$

Eqs. (4.12) and (4.13) are *analytical* approximations for the average and variance of the buckling load, which can be found explicitly for any given two point morphology data $\langle K'K'\rangle$.

To proceed further analytically, and compare the FPM accuracy with previous studies, we use the same common exponential distribution function from (2.7), insert in (4.12) and obtain:

$$\langle \overline{P}_K\rangle \approx 1 + \langle \overline{K}'^2\rangle\cdot(f(\lambda) - 1) = 1 - \rho_K^2\cdot(1 - f(\lambda)), \tag{4.14}$$

where ρ_K if from (2.4) and

$$f(\lambda) = f_1(\lambda) + f_2(\lambda) \tag{4.15}$$

and

$$f_1(\lambda) = \lambda\frac{3 + 20\pi^2\lambda^2 + 32\pi^4\lambda^4(1 - \lambda(1 - \exp(-\lambda^{-1})))}{(1 + 4\pi^2\lambda^2)^2}, \tag{4.16}$$

$$f_2(\lambda) = \lambda^2 \frac{-4((-1)^n e^{-1/\lambda} + 1)}{(n^2-1)(1 + 2(n^2+1)\pi^2\lambda^2 + (n^2-1)^2\pi^4\lambda^4)} + \lambda \frac{2(-1)^n e^{-1/\lambda}\lambda - 1 - \lambda((n-1)^2\pi^2\lambda - 2)}{(n^2-1)(1 + (n-1)^2\pi^2\lambda^2)^2} + \lambda \frac{2(-1)^n e^{-1/\lambda}\lambda - 1 - \lambda((n+1)^2\pi^2\lambda - 2)}{(n^2-1)(1 + (n+1)^2\pi^2\lambda^2)^2}. \quad (4.17)$$

The functions f_1 and f_2 correspond to the effects of the first and second shape functions $w_1(x)$ and $w_2(x)$, respectively. Therefore, two scales are involved in the solution: the morphology scale (λ) and the wavelength of the second buckling shape ($1/n$). To check if they are related, we plot $f_2(\lambda)$, which reflects the influence of w_2 on the solution, for different n values, as seen in Fig. 1. We see that for each n, the maximum effect corresponds to $2\lambda \approx 1/n$, where from (2.7), 2λ is roughly the "grain size". In any case, at $n = 2$ the effect on the buckling load approximation is maximal for any given λ. This suggests that the heterogeneity effects on the buckling loads, is more pronounced through "large wavelength" buckling modes. Therefore, $n = 2$ will be used throughout for the second shape function w_2. Inserting $n = 2$ in (4.17) we obtain:

$$f(\lambda) = \lambda \left[\frac{3 + 20\pi^2\lambda^2 + 32\pi^4\lambda^4(1 - \lambda(1 - \exp(-\lambda^{-1})))}{(1 + 4\pi^2\lambda^2)^2} - \frac{2 + 30\pi^2\lambda^2 + 118\pi^4\lambda^4 - 128\pi^4\lambda^5(e^{-1/\lambda} + 1) + 90\pi^6\lambda^6}{3(1 + 10\pi^2\lambda^2 + 9\pi^4\lambda^4)^2} \right]. \quad (4.18)$$

Note that the function f has the asymptotic properties:

$$f(\lambda \ll 1) = \tfrac{7}{3}\lambda; \quad f(\lambda \to \infty) = 1. \quad (4.19)$$

From (4.13) and (4.14), the COV of $\overline{P}_K$ is found similarly:

$$\bar{\rho}_{P(K)} = \frac{(\mathrm{Var}(P))^{1/2}}{\langle P_K \rangle} = \frac{\sqrt{\langle \overline{K}'^2 \rangle f}}{1 - \langle \overline{K}'^2 \rangle (1 - f)} = \frac{\rho_K \sqrt{f}}{1 - \rho_K^2 (1 - f)}, \quad (4.20)$$

so that

$$\bar{\rho}_{P(K)}(\lambda \ll 1) \approx \rho_K \sqrt{\frac{7\lambda}{3}}. \quad (4.21)$$

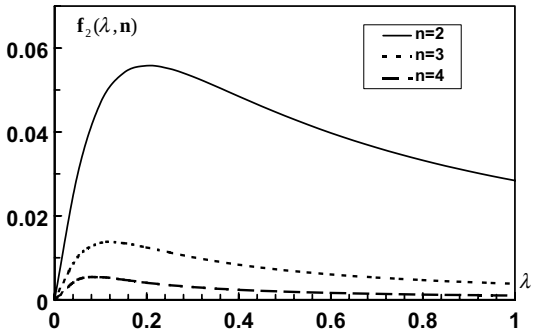

Fig. 1. The effect of f_2, which reflects the influence of w_2 on the solution of the buckling load, as a function of the morphology correlation length λ and n.

5. Comparison with previous studies

Using the procedure of Section 3.2, the FPM can be implemented to many other loading configurations and boundary conditions with no additional difficulty. In this section the validity and accuracy of the method are checked by comparing the results of Section 4 to previous studies by Zhang and Ellingwood (1995) and Garrett (1992). Considering the same values for ρ_K ($=0.3$) and λ ($=0.075$) as Z & E, we obtain from (4.14) and (4.18) the mean buckling loads for a deflection function $w(x)$ having a single term (w_1) and two terms (w_1 and w_2) in the deflection function (4.1):

$$\langle \bar{P}_K \rangle_1 = 0.929; \quad \langle \bar{P}_K \rangle_2 = 0.925. \tag{5.1}$$

The above values are shown in Fig. 2 as two horizontal lines together with the results reprinted from Z & E work, which use the SFE method (second order perturbation SFE) and MCS. It is seen that the present FPM is more accurate than the SFE even when using the first (homogeneous) term only. The excellent fit with the 10,000 MCS results is also noted. When $\lambda \gg 1$, (which means very large grains, or alternatively, perfect two point stiffness correlation) Eq. (4.14) converges to:

$$\langle \bar{P}_K \rangle_{\lambda \to \infty} = 1, \tag{5.2}$$

which agrees with both the MCS and the SFE, as expected, since this is the exact solution. On the other hand, for $\lambda \to 0$ (very small correlation length), (4.14) converges to:

$$\langle \bar{P}_K \rangle_{\lambda \to 0} = 1 - \langle \overline{K}'^2 \rangle = 0.91. \tag{5.3}$$

It is obvious that such a beam behaves homogeneously, with a macro-compliance equal to the average micro compliance, i.e.,

$$S_{\text{eff}} = \frac{1}{K_{\text{eff}}} = \langle S \rangle = \left\langle \frac{1}{K} \right\rangle = \langle K \rangle [1 - \langle \overline{K}'^2 \rangle + \cdots]. \tag{5.4}$$

Thus, (5.3) exhibits the first two terms of a series, which converges to the exact solution for small correlation length if we use higher order FPM terms. The accuracy is limited by the number of correlation points we take in the expansion for P in (3.12). Note that in the SFE and MCS there is a convergence problem for

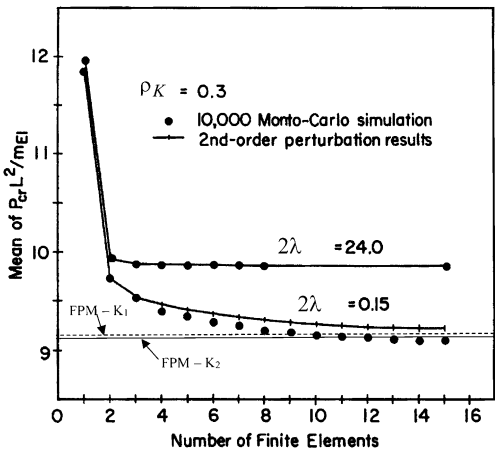

Fig. 2. Average buckling load calculated by (4.12), shown as two horizontal lines, compared to data reproduced from Zhang and Ellingwood (1995). Striped line based on w_1, full line based on w_1 and w_2.

small values of correlation lengths due to numerical problems related to the finite elements size, and therefore Z & E considered $\lambda \geqslant 0.075$ as the lower limit for reliable results. However, the present FPM is analytical and has no limitations of this type.

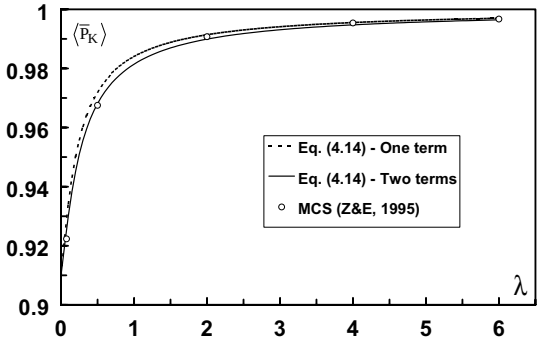

Fig. 3. Average buckling load as a function of the correlation length λ, calculated by (4.12) using one and two deflection shape functions. Solution compared to MCS by Zhang and Ellingwood (1995) ($\rho_K = 0.3$).

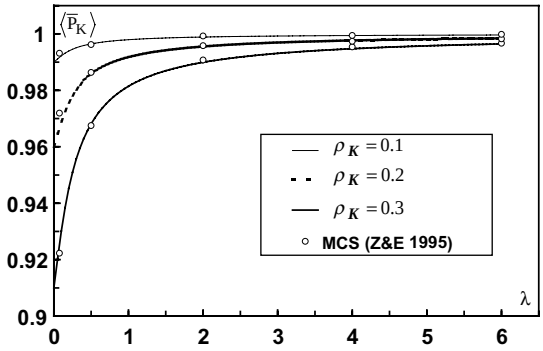

Fig. 4. Average buckling load as a function of the correlation length λ, calculated by (4.12) for different material COV. Solution compared to MCS by Zhang and Ellingwood (1995).

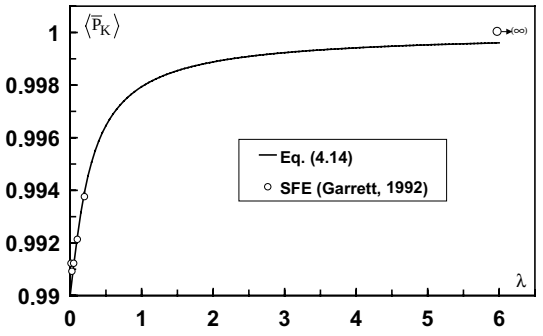

Fig. 5. Average buckling load as a function of the correlation length λ, calculated by (4.12) for $\rho_K = 0.1$. Solution compared to SFE results by Garrett (1992).

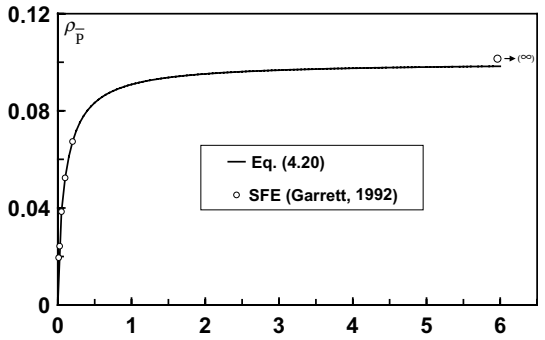

Fig. 6. COV of the buckling load as a function of the correlation length λ, calculated by (4.12). Solution compared to SFE results by Garrett (1992) ($\rho_K = 0.3$).

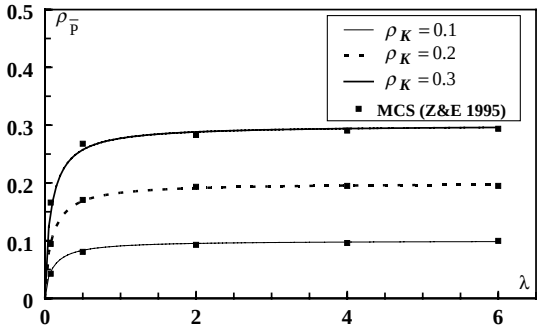

Fig. 7. COV of the buckling load as a function of the correlation length λ, calculated by (4.12) for different ρ_K. Solution compared to MCS by Zhang and Ellingwood (1995).

Fig. 3 shows the FPM solutions using one and two shape functions as a function of λ as compared to the Z & E results with MCS. The effect of the second shape function is small, but distinctive, and the accuracy is good. Notice the discrepancy for the first (smallest λ) MCS point. Figs. 4 and 5 compare the average buckling load by Z & E and Garret's with the two term FPM solutions for three different ρ_K values. Figs. 6 and 7 show the associated comparisons for the buckling COV.

6. Approximations by compliance

So far, the FPM solution was based on the statistical information of the bending stiffness $K(x)$, starting from the elementary homogeneous case for $\langle K \rangle$. This was done since (a) previous studies are all based on stiffness information, and (b) K (and not S^{-1}) is commonly used in the elementary Euler buckling formulas. In the heterogeneous case, $\langle K \rangle$ is the effective value for $\lambda \to \infty$ and $\langle S \rangle^{-1}$ is the exact value for $\lambda \to 0$. It is clear that expansion by S is justified for small λ values, while K is appropriate for large λ values. Therefore, it is useful to examine the FPM solution based on S, and compare it to the one based on K. Recall also that $P(K = \langle K \rangle)$ and $P(S = \langle S \rangle)$ are upper and lower bounds of the average buckling load for any morphology.

Substituting $S = K^{-1}$ in (4.4) and following the FPM procedure through (4.12):

$$P_1 = P_{\langle S\rangle} = \frac{\pi^2}{\langle S\rangle}; \quad P_2 = \frac{n^2\pi^2}{\langle S\rangle}, \tag{6.1}$$

$$P_{,S}|_{\langle S\rangle} = -\frac{2\pi^2 w_1^2}{\langle S\rangle^2}, \tag{6.2}$$

$$P_{,SS}|_{\langle S\rangle} = \frac{8\pi^2}{\langle S\rangle^3}\left[w_1^2 w_1^2 - \frac{1}{n^2-1}(w_1 \circ w_2)(w_1 \circ w_2)\right]. \tag{6.3}$$

Therefore,

$$\langle \overline{P}_S\rangle = \frac{\langle P_S\rangle}{P_{\langle S\rangle}} \approx 1 + 4\langle \overline{S}'\overline{S}'\rangle * *\left[w_1^2 w_1^2 - \frac{1}{n^2-1}(w_1 \circ w_2)(w_1 \circ w_2)\right], \tag{6.4}$$

which is much simpler than (4.12).

The morphology information needed for (4.12) is different from the one for (6.4). From a given data on $\langle K\rangle$ and $\langle K'K'\rangle$ alone, we *cannot* extract the exact values of $\langle S\rangle$ and $\langle S'S'\rangle$ (although approximations can be calculated, as will be shown in the next section). Therefore, in order to compare between the two solutions, we have to choose a definite, fully defined morphology, from which any desired statistical data can be drawn (either by K or S), and calculate these two types of characteristics, each substituted in the proper equation. In addition, in order to use the results obtained above correctly, the chosen morphology should fit its "K appearance" (2.7) too. Note that specific one and two point probabilities of S and K can be "created" by means of more than one specific morphology.

To achieve the above goals, we choose a special 1D "grain like" morphology, for which there is no statistical correlation between the moduli of any two grains, while the modulus inside each grain is uniform. In this case, the two point moduli correlation $\langle K'K'\rangle$ (or $\langle S'S'\rangle$) can be divided into two categories: when the two points are both in the same grain or not. Then,

$$\langle K'K'\rangle = \omega_{\text{in}}\langle K'K'\rangle_{\text{in}} + \omega_{\text{out}}\langle K'K'\rangle_{\text{out}}, \tag{6.5}$$

where ω_{in} is the probability of having the two points in the same grain etc. For the special morphology chosen, we have simply:

$$\langle K'K'\rangle_{\text{in}} = \langle K'^2\rangle; \langle K'K'\rangle_{\text{out}} = 0 \rightarrow \langle K'K'\rangle = \omega_{\text{in}}\langle K'^2\rangle. \tag{6.6}$$

Since ω_{in} is a purely geometric parameter, and $\text{Var}(K)$ is a purely moduli parameter, we can also write for this morphology:

$$\langle S'S'\rangle = \omega_{\text{in}}\langle S'^2\rangle, \tag{6.7}$$

where from (2.7), we take

$$\omega_{\text{in}} = \exp\left(-\frac{|x-X|}{\lambda}\right). \tag{6.8}$$

It is noted that Kröner (1986) used the above method of uncoupling between "micro material" and "micro structure" for calculation of effective moduli of polycrystals.

We now choose as an example, a probability density function $p_K(K)$, which is uniform between two extreme values $(1-\Delta)$ and $(1+\Delta)$ as shown schematically in Fig. 8a. Δ is chosen in such a way that $\rho_K = 0.3$, to fit our previous example. In our case,

$$\langle K\rangle = 1; \quad \langle \bar{K}'^2\rangle = 0.09 = \langle \bar{K}^2\rangle - \langle \bar{K}\rangle^2 = \frac{\Delta^2}{3} \rightarrow \Delta = 0.5196. \tag{6.9}$$

The compliance statistical density $p_S(S)$ is found from $p_K(K)$ by:

$$p_S(S) = p_K(K(S))|K_{,S}|. \tag{6.10}$$

Substituting

$$K = S^{-1}; \quad p_K(K(S))|_{1-\Delta<K<1+\Delta} = \frac{1}{2\Delta}; \quad |K_{,S}| = S^{-2} \tag{6.11}$$

in (6.10), we obtain:

$$p_S(S)|_{(1-\Delta)^{-1}<S<(1+\Delta)^{-1}} = \frac{1}{2\Delta}S^{-2}, \tag{6.12}$$

which is shown schematically in Fig. 8b (note the non-uniformity). Once p_S is known, we calculate the corresponding average and variance of the compliance S (Fig. 8):

$$\langle S\rangle = \int S p_S \,\mathrm{d}S = \frac{1}{2\Delta}\ln\left(\frac{1+\Delta}{1-\Delta}\right) = 1.10814; \quad \langle S^2\rangle = \int S^2 p_S \,\mathrm{d}S = \frac{1}{1-\Delta^2}, \tag{6.13}$$

$$\langle S'^2\rangle = \langle S^2\rangle - \langle S\rangle^2 = \frac{1}{1-\Delta^2} - \left(\frac{1}{2\Delta}\ln\left(\frac{1+\Delta}{1-\Delta}\right)\right)^2 = 0.1419. \tag{6.14}$$

We now have the morphology information needed to calculate the average buckling load using either K (4.12) or S (6.4), such that they both fit the same specific material. The two approximations are shown in Fig. 9, each using the two deflection shape functions (w_1 and w_2). The Z & E results (only two points found for $\lambda < 1$) using SFE method are also given for comparison. All results are normalized to $P_{\langle K\rangle}$, i.e,

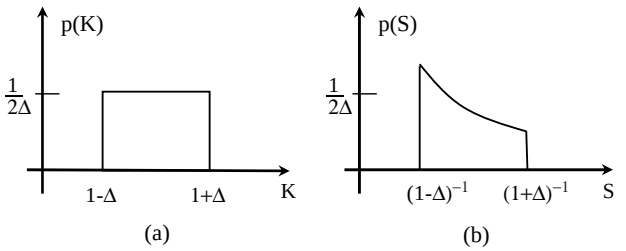

Fig. 8. Moduli probability density function (schematic): (a) stiffness K, (b) compliance S.

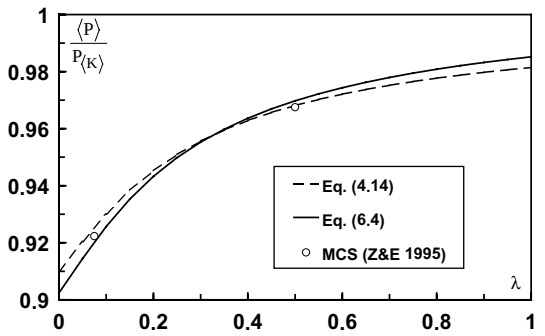

Fig. 9. Average buckling load as a function of the correlation length λ, calculated by stiffness and compliance perturbation (Eqs. (4.12) and (6.4)) ($\rho_K = 0.3$).

$$\frac{\langle P_S\rangle}{P_{\langle K\rangle}} = \frac{\langle P_S\rangle}{P_{\langle S\rangle}}\frac{P_{\langle S\rangle}}{P_{\langle K\rangle}} = \langle \bar{P}_S\rangle\langle K\rangle^{-1}\langle S\rangle^{-1} = 0.902\langle \bar{P}_S\rangle. \tag{6.15}$$

From (6.4), we see that 0.902 is the *exact* buckling load for $\lambda \to 0$, as seen also in Fig. 9.

Further examination of Fig. 9 yields the following:

(1) Solving through K or S, the buckling loads using w_1 and w_2 is always lower than for w_1 only. This is since from the principle of minimum potential energy, additional terms in the deflection function always reduce the buckling load (more degrees of freedom). It means that for a given partial morphology data (for example, $\langle S\rangle$ and $\langle SS\rangle$), we obtain a *conditional upper bound*. However, since $\langle S\rangle$ and $\langle SS\rangle$ do *not* contain the same morphological information as $\langle K\rangle$ and $\langle KK\rangle$, the two conditional bounds cannot be "unified" to a single, better bound.

(2) From the theory of effective moduli (Kröner, 1986) it was shown that exact moduli can be approached either by a stiffness morphology series "from above", or by a compliance morphology series "from below". It means that stiffness based approximations are upper bounds while compliance based approximations are lower bounds for the stiffness. However, these bounds are good for uniform macro stress fields, where boundaries are not present.

(3) From (1) and (2), it is seen that two types of bounds are involved in the present analysis: one is related to the number of deflection shape functions (upper), and the second is related to the type of modulus used (upper for K and lower for S). Therefore, the line based on K in Fig. 9, is a true upper bounds, but the line based on S is not a bound. Nevertheless, the "S" line is more accurate as λ approaches zero.

7. Accuracy consideration for general morphology

In Section 6, buckling of a beam with a specific morphology was examined, for which the full statistical information (point probabilities) is known. We could therefore study approximate solutions either through S or K. This would be the case for any other "fully given" morphology. In these cases, our homogeneous "starting point" controls the solution accuracy. However, in many cases, we have only partial morphological information, which reduces the accuracy.

Consider for example, the case where only $\langle K\rangle$ and $\langle K'K'\rangle$ are known from measurements, but $\langle S\rangle$ and $\langle S'S'\rangle$ are needed for buckling calculations, as for the case $\lambda > 1$. Functional expansion yields:

$$S = S|_{\langle K\rangle} + S_{,K} * K' + S_{,KK} * K'K' + \cdots, \tag{7.1}$$

where all derivatives are calculated at $\langle K\rangle$. Therefore,

$$\langle S\rangle = S|_{\langle K\rangle} + S_{,KK} * \langle K'K'\rangle + \cdots. \tag{7.2}$$

We see when only partial information on K is known, even $\langle S\rangle$ cannot be found accurately. Subtracting (7.1) from (7.2) we obtain:

$$\langle S'S'\rangle = \langle (S_{,K} * K')(S_{,K} * K')\rangle + \cdots \cong S_{,K} * \langle K'K'\rangle * S_{,K}. \tag{7.3}$$

Thus, both $\langle S\rangle$ and $\langle SS\rangle$ are accurate up to the $\langle KK\rangle$ order. This is in contrast to the case, where they are measured directly, and are exact. Using the relation $S = K^{-1}$ we obtain:

$$S|_{\langle K\rangle} = \langle K\rangle^{-1}; \quad S(x_1)_{,K(x_2)}|_{\langle K\rangle} = -[K(x_1)]^{-2}\delta(x_1 - x_2). \tag{7.4}$$

Inserting (7.4) in (7.3), and using the Dirac properties yields:

$$\langle S'S'\rangle = \langle K\rangle^{-4}\langle K'K'\rangle + \cdots, \tag{7.5}$$

which is the best accuracy we can achieve if only $\langle K\rangle$ and $\langle K'K'\rangle$ are given. Thus, it is expected that using (7.5) and (7.4a) instead of the measured values of $\langle S\rangle$ and $\langle S'S'\rangle$ will reduce the accuracy. However, if we derive our calculation up to the "two point correlation", the *order* of accuracy is not expected to change. We can therefore draw a general conclusion, that the accuracy of the FPM solution is of the order of $\langle K'^2\rangle$ for all λ, values, independent of our "source data", coming from S or K. A more accurate statement will be possible for every private case.

There is still the basic interesting problem of finding the best value of the homogeneous solution, around which the most accurate solution is expected by the FPM for a given number of perturbation terms. This is an optimization problem, which is currently under investigation.

8. Clamped-free beam and symmetry considerations

In homogeneous beams, the clamped-free (C-F) buckling load can be obtained directly from the solution of the simply supported (S-S) case by symmetry conditions. However, if the bending stiffness is stochastic, the symmetry is not valid, as seen above by the contribution of the second $(w_2(n=2))$ non-symmetric shape function. Therefore, it is interesting to study the difference between the two cases, originating from a net morphology effect.

Assuming again a deflection shape $w(x)$ of the C-F beam of length $L=1$ as a series of which the first term has the shape function of the homogeneous solution, we have:

$$w(x) = A_1 w_1(x) + A_2 w_2(x) = A_1\left(1-\cos\left(\frac{\pi x}{2}\right)\right) + A_2\left(1-\cos\left(\frac{3\pi x}{2}\right)\right), \tag{8.1}$$

where the two boundary conditions at the fixed end $(x=0)$ are satisfied. Note that the minimal n for the second term is $n=3$, and not $n=2$ as for the S-S case. Recalling that the contribution of each term diminishes as n increases, we expect the effect of w_2 in the C-F case to be smaller than for the S-S case.

The deflection of the beam at $x=1$ is (A_1+A_2), so the moment distribution along the beam is:

$$M(x) = P(A_1+A_2-W) = P\left(A_1\cos\left(\frac{\pi x}{2}\right) + A_2\cos\left(\frac{3\pi x}{2}\right)\right). \tag{8.2}$$

Performing the same FPM procedures as for the S-S case, with the same two point probability function for the stiffness (2.7), the average buckling load is obtained as:

$$\langle \overline{P}_K\rangle = 1 + \langle \overline{K}'^2\rangle \cdot (f(\lambda)-1) = 1 - \rho_K^2\cdot(1-f(\lambda)), \tag{8.3}$$

where:

$$\langle \overline{P}_K\rangle = \frac{\langle P_K\rangle}{P_{\langle K\rangle}}; \quad P_{\langle K\rangle} = \frac{\pi^2\langle K\rangle}{4}, \tag{8.4}$$

$$f(\lambda) = \lambda\left[\frac{3-4\lambda+5\pi^2\lambda^2-4\pi^2\lambda^3(1-\exp(-\lambda^{-1}))+2\pi^4\lambda^4-2\pi^4\lambda^5(1-\exp(-\lambda^{-1}))}{(1+\pi^2\lambda^2)^2} + \frac{-2+4\lambda-15\pi^2\lambda^2+4\pi^2\lambda^3(3e^{-1/\lambda}+5)+33\pi^4\lambda^4+2\pi^4\lambda^5(15e^{-1/\lambda}+17)-20\pi^6\lambda^6}{16(1+5\pi^2\lambda^2+4\pi^4\lambda^4)^2}\right]. \tag{8.5}$$

The COV of the buckling load is:

$$\rho_P = \frac{\rho_K \sqrt{f}}{1 - \rho_K^2 \cdot (1 - f)}. \tag{8.6}$$

Figs. 10 and 11 show the influence of λ and ρ_K on the mean and COV of the critical buckling load for a C-F column, compared to the simply supported case. For the average buckling load, we examine the parameters

$$\Delta_P = 4\langle \overline{P}_K \rangle_{\mathrm{CF}} / \langle \overline{P}_K \rangle_{\mathrm{SS}} - 1, \tag{8.7}$$

and for the COV:

$$\Delta_\rho = 1 - \langle \bar{\rho}_P \rangle_{\mathrm{CF}} / \langle \bar{\rho}_P \rangle_{\mathrm{SS}}. \tag{8.8}$$

It is seen from Fig. 10 that the morphology effects vanish for $\lambda = 0$ and $\lambda \gg 1$ as expected. The CF average buckling load is relatively larger than for the SS case. The reason is that when we "compose" an SS beam of length 2 by two CF beams of length 1, the morphology in the double CF beam is symmetric,

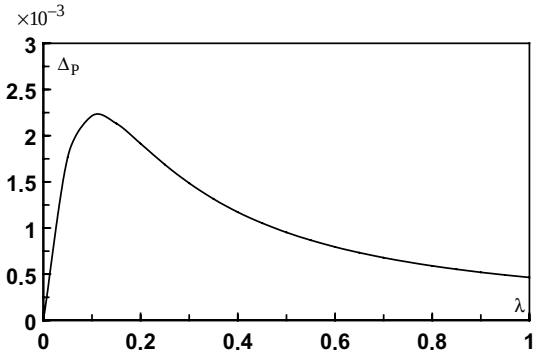

Fig. 10. ΔP as a function of λ (Eq. (8.7)). Δp reflects the relative difference in the average buckling load between a SS and CF beams due to morphology ($\rho_K = 0.3$).

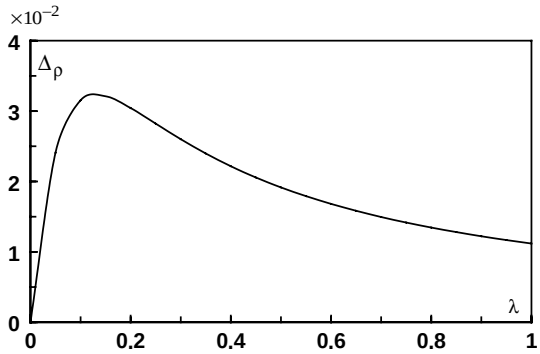

Fig. 11. $\Delta\rho$ as a function of λ (Eq. (8.8)). $\Delta\rho$ reflects the relative difference in the COV of the buckling load between a SS and CF beams due to morphology ($\rho_K = 0.3$).

meaning larger correlation length and higher buckling loads. The effect is maximal at a grain size of $2\lambda \approx 1/4$.

Fig. 11 shows similar behavior for the statistical dispersion of the buckling load, which is slightly smaller for the CF case. The reason is that the CF column is "enforced" to buckle in a "half symmetric" shape.

9. Conclusions

The FPM, developed here for buckling problems, was found to be more accurate than the SFE method, and have no accuracy problems for small correlation lengths.

The advantages of the present FPM method is that, with the common (small deviation) limitation of any perturbation scheme, the solutions are analytical, easy for calculation and provide an additional insight, which is difficult to achieve by SFE or MCS methods.

Any perturbation method is limited in its accuracy to a relatively small region near the chosen parameter or function. Therefore, care should be taken when using the method for the whole range of the correlation length λ. Using the FPM separately near $\langle K \rangle$ and $\langle S \rangle$, showed how the first is more appropriate for $\lambda > 1$ and the second is more suitable for $\lambda < 1$. An accurate solution for the intermediate region ($\lambda \sim 1$) is still in demand. Moreover, the general problem of finding the best "homogeneous" material properties, to be used as a zero order term for the heterogeneous case is a fundamental optimization problem, which deserves a separate study.

The accuracy of the FPM is strongly related to the accuracy of the homogeneous (first term) shape function. In many cases, an exact solution for the homogeneous case is available, and can be used for the heterogeneous case. In more complex structures, where analytical solutions are not available, the homogeneous problem can be solved by any chosen approximate (numerical) method. Then, the homogeneous shape function can be used as a first term in the FPM solution for the heterogeneous case.

The second order functional perturbation leads to a quadratic equation for the buckling load (4.4), which can be solved analytically. This will not be the case when higher order morphology data is needed. Fortunately, the higher order accuracy is not frequently needed in engineering practice.

Finally, it should be noted that practical structures are much more complicated, while a direct use of FPM is clearly limited to simple problems. This gap can be closed in the future by implementing the FPM for stochastically heterogeneous structures into regular FE programs.

Acknowledgement

This research was partially supported by the Israeli Science Foundation, 2002.

References

Altus, E., 2001. Statistical modeling of heterogeneous microbeams. Int. J. Solids Struct. 38 (34–35), 5915–5934.

Altus, E., Givli, S., 2002. Strength reliability of statistically heterogeneous microbeams. Int. J. Solids Struct. 40 (9), 2069–2083.

Beran, M., 1968. Statistical Continuum Mechanics. Interscience Publishers.

Elishakoff, I., 2000. Uncertain buckling: Its past, present and future. Int. J. Solids Struct. 37 (46–47), 6869–6889.

Elishakoff, I., 2001. Inverse buckling for inhomogeneous columns. Int. J. Solids Struct. 38, 457–464.

Garrett, D.J., 1992. Critical buckling load statistics of an uncertain column, probabilistic mechanics and structural and geotechnical reliability. In: Proceedings of the Sixth Specialty Conference, ASCE, Denver, CO, July 8–10, pp. 563–566.

Graham, L.L., Siragy, E.F., 2001. Stochastic finite-element analysis for elastic buckling of stiffened panels. J. Engrg. Mech. 127 (1), 91–97.

Graham, L., Deodatis, G., 1998. Variability response functions for stochastic plate bending problems. Structural Safety 20, 167–188.
Graham, L.L., Deodatis, G., 2001. Response and eigenvalues analysis of stochastic finite element systems with multiple correlated material and geometric properties. Probab. Engrg. Mech. 16 (1), 11–29.
Kröner, E., 1986. Statistical modelling. In: Gittus, J., Zarka, J. (Eds.), Modeling Small Deformation of Polycrystals. Elsevier, pp. 229–291.
Ramu, S.A., Ganesan, R., 1994. Response and stability of stochastic beam-column using stochastic FEM. Comp. Struct. 54 (2), 207–221.
Shinozuka, M., Astill, J.C., 1972. Random eigenvalue problems in structural analysis. AIAA J. 10 (4), 456–462.
Zhang, J., Ellingwood, B., 1995. Effects of uncertain material properties on structural stability. J. Struct. Engrg. 121 (4), 705–716.